Advanced Materials Interfaces

ADVANCED MATERIALS INTERFACES Open Access

www.advmatinterfaces.de

RESEARCH ARTICLE OPEN ACCESS

Charge Injection for Polarization Screening at Electrode Interfaces and the Antiferroelectric Double Hysteresis Loop of La-Doped Pb(Zr,Sn,Ti)O_3

Binxiang Huang[1] | Pengcheng Hu[1] | Melissa A. Larsson[1] | Johanna Steinmann[1] | Tongqing Yang[2] | Tadej Rojac[3] | Andreas Klein[1]

[1]Technische Universität Darmstadt, Institute of Materials Science, Electronic Structure of Materials, Darmstadt, Germany | [2]Functional Materials Research Laboratory, Tongji University, Shanghai, China | [3]Electronic Ceramics Department, Jožef Stefan Institute, Ljubljana, Slovenia

Correspondence: Andreas Klein (aklein@esm.tu-darmstadt.de)

Received: 23 July 2025 | **Revised:** 23 November 2025 | **Accepted:** 7 December 2025

Keywords: antiferroelectric | electrodes | ITO | polarization | PZT | $RuO_2$${\rm RuO}_2$ | screening | X-ray photoelectron spectroscopy

ABSTRACT

Polarization screening at electrode interfaces has been the subject of controversial studies. The nature and role of the screening charges, especially when comparing the behavior of ferroelectric and antiferroelectric materials, are still not entirely clear. In this study, we analyze the polarization screening at electrode interfaces of ferroelectric and antiferroelectric La-doped $PbZr_{0.75}Sn_xTi_{0.25-x}O_3$ by X-ray photoelectron spectroscopy with in situ polarization reversal. A variation of the Schottky barrier height at a few nanometer thick RuO_2 and Sn-doped In_2O_3 electrode interfaces, which is caused by an imperfect screening of the polarization, is only observed for samples exhibiting ferroelectricity but not for samples with antiferroelectric hysteresis loops. According to the line shape analysis of the photoelectron spectra, the different screening behavior of ferroelectric and antiferroelectric La-doped $PbZr_{0.75}Sn_xTi_{0.25-x}O_3$ can be assigned to differences in charge injection. Antiferroelectric hysteresis loops are observed if the screening charges are completely injected from the electrode while only partial charge injection is observed into ferroelectric samples. Charge injection could be fundamental to the reversibility of the field-induced transition from the non-polar to the polar state of antiferroelectrics.

1 | Introduction

The high recoverable energy density of antiferroelectric capacitors, which results from the specific double hysteresis loop depicted in Figure 1b, is particularly suitable for efficient electric energy converters in grid systems and electric vehicles [1]. The characteristic double hysteresis loop of ferroelectrics is ascribed to a reversible electric field-induced phase transition between a non-polar and a polar phase of the material having similar energy [2]. The polar state is stabilized by the electric field, and a removal of the electric field transfers the material back into the non-polar state without remanent polarization. The energies of the non-polar and polar phases and their respective dependencies on the electric field are (bulk) properties of the materials. By studying the screening of polarization at interfaces with thin electrodes by means of X-ray photoelectron spectroscopy (XPS) with in situ application of electric fields, it will be demonstrated that the shape of the hysteresis loop of La-doped $PbZr_{0.75}Sn_xTi_{0.25-x}O_3$, the prototype (anti)ferroelectric compound [1], is related to an interfacial property. Measurements of samples with tiny variation in composition or temperature and with different electrode materials reveal a different screening behavior of the polarization at the electrode interface. The screening charges of samples exhibiting a ferroelectric hysteresis loop remains at least partially

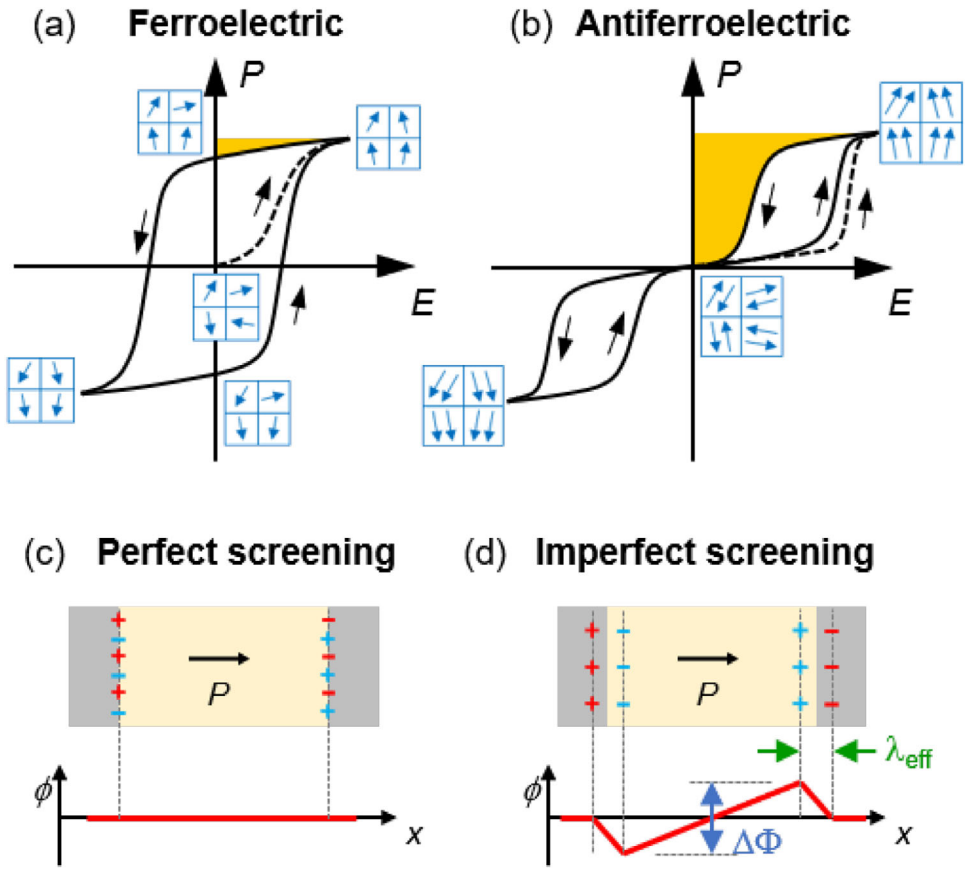

FIGURE 1 | Polarization, P vs. electric field, E, hysteresis loops of a ferroelectric (a) and an antiferroelectric (b) compound with schematic orientation of microscopic electric dipole moments (arrows) and domains (squares). The dashed lines represent the initial cycle for unpoled materials. The recoverable energy density is indicated by the yellow areas. Perfect and imperfect screening of polarization at electrode interfaces are schematically depicted in (c) and (d). Imperfect screening is described by an effective screening length, $\lambda_{\mathrm{eff}} \approx 1$ Å, which can be taken as an effective separation of the ferroelectric bound charges (blue) and the screening charges in the electrode (red) [3]. For finite values of λ_{eff}, imperfect screening induces a variation of the electrostatic potential resulting in a variation of the Schottky barrier height with polarization of $q_e \cdot \Delta\Phi$, where q_e is the elementary charge.

on the electrode. In contrast, the charges screening the polarization in the high-field ferroelectric state of samples exhibiting a double hysteresis loop are injected from the electrode into the substrate.

Screening of polarization charges at interfaces is fundamental to maintain the remanent polarization of ferroelectric materials [4–6]. Uncompensated bound charges would generate a depolarizing field, which will completely suppress polarization. The case of perfect screening of polarization at an interface between a ferroelectric and a conducting electrode can schematically be described by coinciding positions of the bound polarization charges and the screening charges as depicted in Figure 1c. However, the screening of polarization is imperfect in most cases. This results in the variation of the electrostatic potential across the sample as illustrated in Figure 1d. One consequence of an imperfect screening is the widely observed reduction of the capacitance of ferroelectric thin films with reducing film thickness, typically denominated as the introduction of a dead layer [7]. As the effective screening length, λ_{eff}, i.e., the effective separation between the bound and the screening charges, is typically of the order of an Angstrom [3, 8] and thereby shorter than the inelastic mean free path of the photoelectrons in an XPS experiment, the presence of imperfect screening can be directly observed from the polarization dependence of the Schottky barrier height at the ferroelectric/electrode interface, $\Delta\Phi$ [9–11].

The situations for perfect and imperfect screening at electrode interfaces, illustrated in Figure 1c,d assume that the screening charges are located on the electrode. The only difference is the very small spatial separation of the bound and the screening charges. In other words, the ferroelectric polarization reaches up to the electrode and then drops abruptly. The situation becomes different if the screening charges do not remain in the electrode but are injected into the substrate. In this case, the polarization will not reach the electrode as outlined by Kretschmer and Binder [12, 13]. The number of charges required to switch polarization does not depend on the location of the charges, i.e. if they are injected into the dielectric or remain on the electrode. Several observations related to ferroelectric thin films, such as imprint and fatigue have actually been related to the injection of the screening charges from the electrodes [14–22]. It is noted that the injection of charges, which screen the bound polarization charge is distinguished from the charges contributing to the leakage current. Screening charges are limited, and they will be immobilized (trapped) at the plane terminating the polarization. In contrast, charges contributing to the leakage current are permanently injected and remain mobile, even if they are trapped

intermediately in a hopping transport. Leakage currents are not measurable with the samples studied in this work due to the high thickness of > 100 μm. The situation is different for thin films, where the total resistance of the material is orders of magnitude lower and electric fields are typically higher. Due to the higher fields, injection barriers are also reduced by the image charge effect, leading to substantial leakage currents of thin films [23, 24]. Injection into thin films can further be enhanced by inserting a very thin low permittivity dielectric layer between the ferroelectric layer and the electrode [25–28]. In any case, the effects evaluated in this contribution are not affected by charges injected from the electrode, which contribute to the leakage current.

This contribution describes experimental observations on ferroelectric and antiferroelectric bulk ceramics with RuO_2 and Sn-doped In_2O_3 (ITO) electrodes with a few nanometer thickness. The experimental setting enables to monitor the changes of the Schottky barrier heights at the electrode interfaces and changes of the carrier concentration in the ITO electrodes with applied electric field. Pronounced differences of charge injection behavior depending on ferroelectric and electrode material are revealed.

2 | Results

Ferroelectric hysteresis loops recorded on the sample stage of the XPS system with Pt bottom and either RuO_2 or ITO top electrodes are displayed in Figure 2a–c. The PLZST samples studied in this work contain 75% Zr and a varying amount of Ti and Sn on the *B*-site of the perovskite lattice. The samples are doped with 2% La on the *A*-site. At room temperature, samples with 11% Ti (denominated as C11) exhibit reversible ferroelectric hysteresis loops with a saturation polarization of 32 μC/cm^2 for RuO_2 and 33.7 μC/cm^2 for ITO and coercive fields of 0.8 kV/mm for RuO_2 and 1.2 kV/mm for ITO, respectively (see Figure 2b). Samples with 9% Ti (denominated as C09) exhibit an antiferroelectric double hysteresis loop at room temperature as depicted in Figure 2c. The saturation polarization at high electric fields is comparable to the ferroelectric C11 sample. For reference, a ferroelectric $Pb(Zr,Ti)O_3$ sample (PIC 151 from PI ceramic, Lederhose, Germany) is used throughout this work. It is noted that significantly higher electric fields are required to induce the ferroelectric state of the C11 sample in the first cycle. This behavior is different from that of the ferroelectric reference sample and indicates an irreversible transition from a non- or antipolar ground state into a ferroelectric state. In contrast, the ferroelectric reference sample has a polar ground state from the beginning.

Pb $4f_{7/2}$ x-ray photoelectron spectra of a PIC 151, and two PLZST samples containing 11 and 9% Ti with RuO_2 and ITO top electrodes are given in dependence on applied electric field in panels (d–i) in Figure 2. RuO_2 and ITO differ in work function by about 1.1 eV [30, 31], resulting in a similar difference of the Fermi level at the interface [32]. The different Fermi levels are confirmed by the different binding energies of the Pb $4f_{7/2}$ emission with RuO_2 and ITO electrodes (see black lines in panels (d) and (g) for PIC 151, (g) and (h) for C11, and (f) and (i) for C09 in Figure 2). It is mentioned that the electronic structures of ITO and RuO_2, and hence the Schottky barrier heights at the interface are fully developed at a film thickness of 3 nm [33]. Therefore, the thickness of the layers does not effect the determination of the barrier height.

For the ferroelectric PIC 151 reference sample, the Pb $4f$ emission is shifting in dependence on the electric field, indicating an imperfect screening of polarization. Changes in peak shape, which are more pronounced in the case of the ITO top electrode, will be discussed later. For C11, the Pb $4f$ peak still shifts with polarization for the RuO_2 top electrode. With the ITO top electrode, the maximum of the Pb $4f$ emission does not change with polarization, but a pronounced asymmetry develops on the low binding energy side of the Pb $4f$ emission for positive polarization (negative polarity at ITO electrode). In contrast, the antiferroelectric C09 sample exhibits a completely different behavior. No shifts and no changes of peak shape are observed for the Pb $4f$ emission of the antiferroelectric C09 sample with both electrode materials, indicating a different screening behavior. Ru $3d$ photoelectron spectra recorded from the three different samples in dependence on applied electric field are provided together with the associated Pb $4f$ spectra in the Supporting Information. No changes in the Ru $3d$ emissions are observed. The changes of the In $3d$ emissions displayed in Figure 2i–l are discussed later.

A different screening behavior of the antiferroelectric sample as compared to the ferroelectric ones is corroborated by measuring a sample containing 11% Ti at different temperatures. The recorded hysteresis loops and Pb $4f_{7/2}$ spectra of a sample with a RuO_2 top electrode are depicted in Figure 3 for i) initial measurement at room temperature, ii) subsequent measurement at 100°C, and iii) measurement performed after subsequent cooling to room temperature (Ru $3d$ spectra are provided in the Supporting Information). The Pb $4f$ peaks exhibit clear binding energy shifts upon polarization reversal in the ferroelectric states at room temperature before and after measurement at 100°C. In contrast, no changes in peak shape and binding energy are observed in the antiferroelectric state at 100°C. A reference experiment performed with a ferroelectric PIC 151 sample revealed no difference in screening behavior between room temperature and 100°C. As presented in the Supporting Information, the Pb $4f$ emission shifts with polarization in both cases. The temperature dependent behavior strongly suggests that the different screening is driven by the (anti)ferroelectric ordering and not by a different chemical composition.

3 | Discussion

The behavior of the Pb $4f$ emission indicates a different polarization screening of ferroelectric and antiferroelectric compounds. Such differences are expected between perfect and imperfect screening of polarization as illustrated in Figure 1. However, such a scenario does not apply to the present case. The effective screening length, which relates to the difference between perfect and imperfect screening, depends on the atomic arrangement at the interface [3]. It is not expected that this arrangement is significantly different for samples differing by only 2% in Ti content (C09 vs. C11). The structural analysis (see Supporting Information) also reveals no difference between C09 and C11 in the unpoled state, in which the interfacial bonds are established.

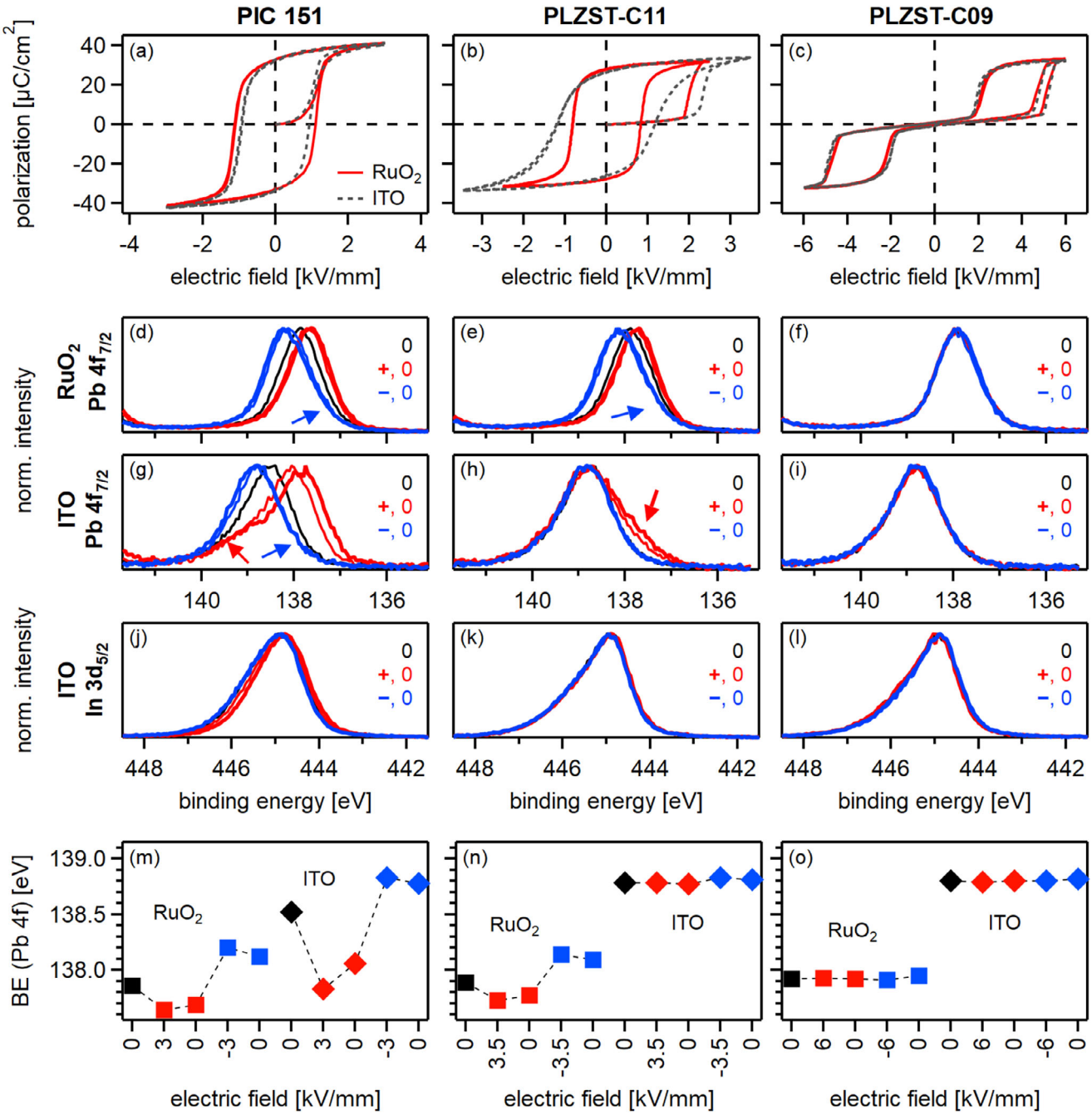

FIGURE 2 | Polarization hysteresis loops of a ferroelectric PIC 151 reference sample (a), a 2% La-doped $PbZr_{0.75}Sn_{0.14}Ti_{0.11}O_3$ (C11) (b) and a 2% La-doped $PbZr_{0.75}Sn_{0.16}Ti_{0.09}O_3$ (C09) (c) measured in ultrahigh vacuum on the sample stage of the photoelectron spectrometer with thin RuO_2 or ITO top electrodes. Pb $4f_{7/2}$ XP spectra measured through RuO_2 top electrodes are given in (d–f), those measured through ITO top electrodes in (g–i). In $3d_{5_2}$ spectra of samples with ITO top electrode are given in (i–l) and peak maximum positions of the Pb $4f$ emissions in (m–o). The labels in panels (d–l) indicate the polarity of the voltage at the top electrode. Thick red and blue lines in (d–l) are with applied voltage (+, −) and thin lines after removal of the voltage (0). The magnitude of the voltage corresponds to the maximum electric field of the polarization loops of the respective sample. Arrows in (d,e,g,h) indicate asymmetric peak shapes. The Fermi level positions with respect to the valence band maximum at the interfaces can be extracted from the Pb $4f$ binding energies in (m–o) by subtracting 136.5 eV [29].

It is even less likely that the atomic arrangement changes significantly when a sample is heated from room temperature to 100°C. In this case, the composition of the sample and the interface for the ferroelectric state at room temperature and the antiferroelectric state at 100°C will be identical. Therefore, the different screening behavior likely has a different origin.

The In $3d$ spectra, which are displayed in Figure 2j–l of the samples with ITO electrodes, hint toward a potential explanation for the differences. The In $3d$ spectra from the ferroelectric PIC 151 reference sample exhibit clear binding energy shifts and changes in peak shape upon polarization reversal. Higher binding energies and the more asymmetric peak shape of the In $3d$ emission, which are observed for the negatively polarised ITO

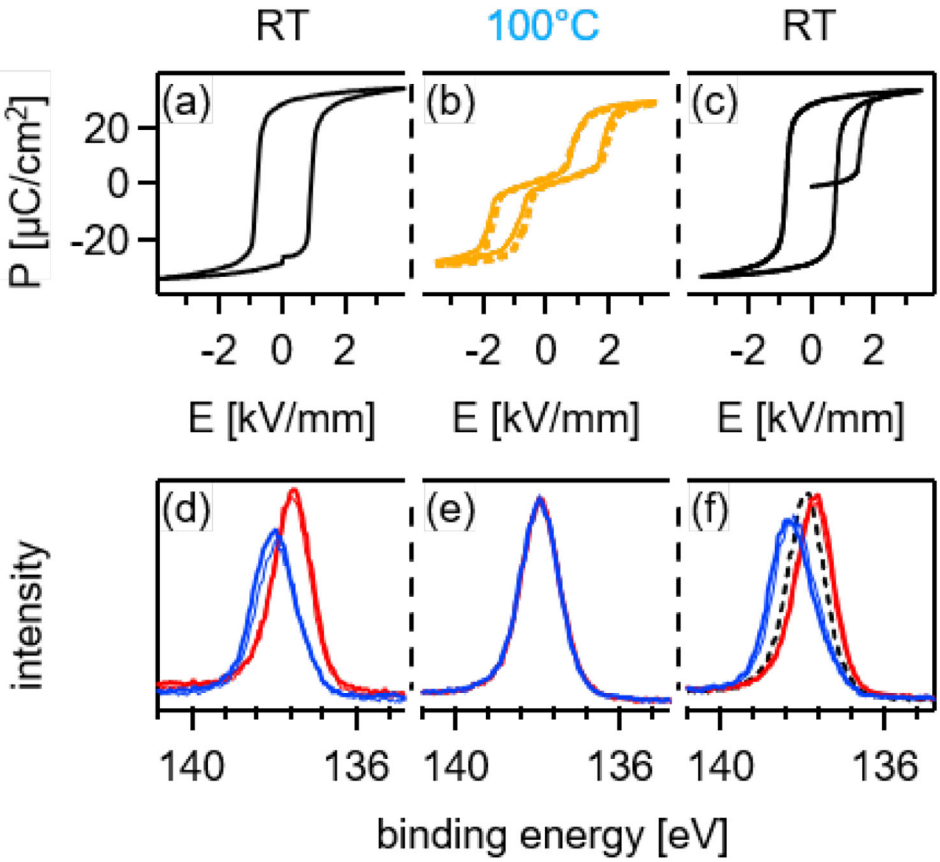

FIGURE 3 | Polarization hysteresis loops of PLZST sample containing 11% Ti on the *B*-site measured on the sample stage of the spectrometer at room temperature (a), at 100°C (b) and after cooling to room temperature (c). Respective Pb $4f_{7/2}$ spectra are given in panels (d–f) measured with an applied electric field of +3.5 kV/mm (thick red lines), 0 (thin red lines), −3.5 kV/mm (thick blue lines) and 0 kV/mm (thin blue lines), respectively. The dotted black spectra in (f) has been measured without an electric field directly after cooling to room temperature.

electrode, are both related to a higher carrier concentration in the ITO film [34]. It can thus be excluded that the shift is induced by charging during the photoemission process. Evidently, the ITO layer has a higher electrical conductivity when negatively polarized and a lower conductivity when positively polarized. The changes of the In 3*d* peak of the PIC 151 samples are remanent, they persist after removal of the electric field, indicating that the changes are not related to the applied voltage but to the change of polarization.

A noticeable change of the electrode's carrier concentration upon polarization reversal is expected for semiconducting electrode materials if the screening charges are located in the electrode as illustrated in Figure 4 [35, 36]. The effect is negligible for metallic electrodes and therefore not observed for the RuO_2 electrodes. However, it can clearly be identified for the semiconducting ITO electrodes. For negative polarization, additional electrons are inserted into the electrode from the outer circuit. These screening charges are mobile and hence contribute to the free electron concentration. ITO films typically have carrier concentrations of $5-10\times10^{20}$ cm^{-3} if prepared with conditions similar to those used in this work [37]. For a film thickness of 5 nm, this corresponds to a (sheet) density of electrons of $2.5-5\times10^{14}$ cm^{-2}. This is of similar magnitude as the density of screening charges corresponding to a polarization of 40 μC/cm^2, which equals 2.5×10^{14} cm^{-2}. Hence, if all the screening charges remain on the electrode, almost all electrons would have to be removed from the electrode to compensate for the polarization in the case of positive polarization of the ITO electrode. Such a scenario is not realistic, as the symmetric PE-loops recorded with ITO electrodes would not be possible if the ITO conductivity is strongly suppressed. The effect of a varying conductivity of thin ITO electrodes on the polarization hysteresis loop is illustrated in the Supporting Information for the case of $BaTiO_3$ single crystals and polycrystalline $Pb(Mg_{1/3}Nb_{2/3})O_3$-$PbTiO_3$ (PMN-PT) bulk ceramics. Both materials exhibit pronounced asymmetric hysteresis loops and changes of the In 3*d* spectra, which can be explained by changes of the electrode's conductivity. Therefore, the symmetric hysteresis recorded for PIC 151, C09, and C11 with thin ITO top electrodes (black dotted lines in Figure 2a–c) can only be explained if at least part of the screening charges are injected into the (anti)ferroelectric bulk.

The presence of charge injection is corroborated by the binding energies of the Pb 4*f* emissions in Figure 2, which are displayed in Figure 2m–o. As already mentioned above, the binding energies of the Pb 4*f* before poling the sample (black spectra in Figure 2d–i and black symbols in Figure 2d–f), which corresponds to the initial Fermi level position inside the energy gap (the Schottky barrier at the interface), is different for RuO_2 and ITO. Taking the initial state as reference, the Pb 4*f* emissions of the PIC 151 and C11 samples exhibit a smaller shift to lower binding energies for

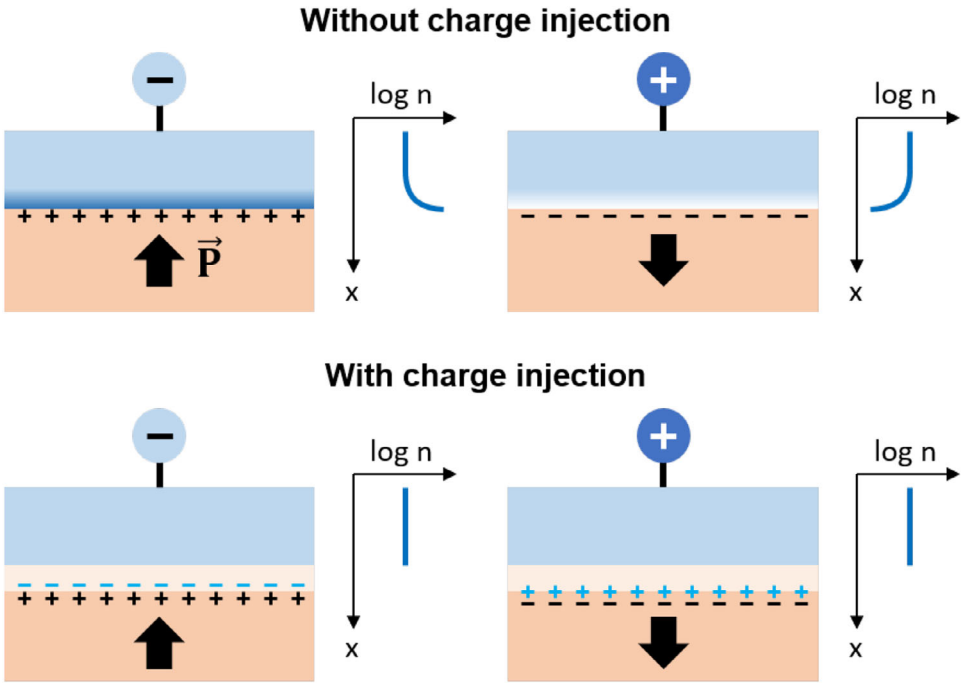

FIGURE 4 | Changes of electron density in an ITO electrode upon polarization reversal without charge injection and with charge injection.

the RuO_2 electrode and a smaller shift to higher binding energies for the ITO electrode. In other words, if the Fermi level is already low/high at the interface, the shift to lower/higher binding energy upon poling the samples is less pronounced. Assuming that the magnitude of the shift is related to charge injection (no shift for complete injection of screening charges), this indicates that injection of holes is easier for lower Fermi levels (RuO_2 electrode) and injection of electrons is easier for higher Fermi levels (ITO electrodes). This is the expected behavior for charge injection.

Assuming different charge injection from RuO_2 and ITO electrodes, the asymmetric peak shapes of the Pb 4*f* emissions in Figure 2, which are indicated in Figure 2 by red and blue arrows, can be rationalized. The asymmetric peak shapes are likely related to an inhomogeneous electrostatic potential at the interfaces, i.e. a variation of the Schottky barrier height. This variation is induced as XPS is a local probe of the electrostatic potential and a variation of the potential in the probed area results in a distribution of binding energies according to the distribution of the potential [38]. As an example, the Pb 4*f* emission of the PIC 151 specimen with an ITO electrode is considered. The peak is quite symmetric at high binding energy for negative voltage polarity (blue spectra in panel (g) of Figure 2. For positive voltage polarity, where injection of holes is expected but difficult because of the high Fermi level of the ITO electrode, a part of the peak is not shifting but remaining at high binding energy, representing parts of the surface where charge injection occurs (it is not expected that the absence of the shift is caused by an absence of polarization switching as the saturated polarization is comparable for RuO_2 and ITO interfaces). The majority of the peak is shifting to lower binding energy, representing parts of the interface where screening charges are not injected but remain on the electrode and induce peak shifts due to imperfect screening. The situation is similar at the C11/ITO interface. In this case, the majority of the surface exhibits charge injection.

The experimental approach employing X-ray photoelectron spectroscopy with thin (semiconducting) electrodes and in situ polarization reversal can clearly reveal insights into charge injection at (anti)ferroelectric/electrode interfaces. In the studied cases of $Pb(Zr,Ti)O_3$ related compounds, charge injection is evidently present for all materials, particularly for the low work function ITO electrodes. Binding energy shifts of the Pb 4*f* emissions induced by imperfect screening of polarization are completely absent in the antiferroelectric state, regardless of whether this is induced by composition or temperature variation. This suggests that the antiferroelectric double hysteresis loop is directly connected to charge injection. One speculation is that charge injection might be beneficial for the removal of polarization upon reduction of the electric field. When the ferroelectric state will not reach the electrode, no nucleation of an antiferroelectric state is required to switch back from the ferroelectric to the antiferroelectric state, as discussed in literature [20]. On the other hand, it might also be possible that screening charges remaining in the electrode contribute to the stabilization of ferroelectric polarization after removal of the applied voltage. Further experimental and/or theoretical studies are required, however, to further establish such a connection.

The performed experiments do not reveal details of the charge injection mechanism. It remains unclear, for example, if the charges are injected into the valence and conduction band via thermal Schottky emission or directly into trap states. Charges in the energy bands would be rather mobile, which is not expected given the very high resistivity of donor-doped PZST [29]. The potential barriers for injection into the valence and conduction band extracted from the binding energies of the Pb 4*f* peaks are also rather high. Taking a distance between the Pb 4*f* peak and the valence band maximum of 136.5 eV [29], the barrier for hole injection into the valence band is extracted from Figure 2m–o as $\geq$ 1.1 eV, in good agreement with previous work [33]. Assuming

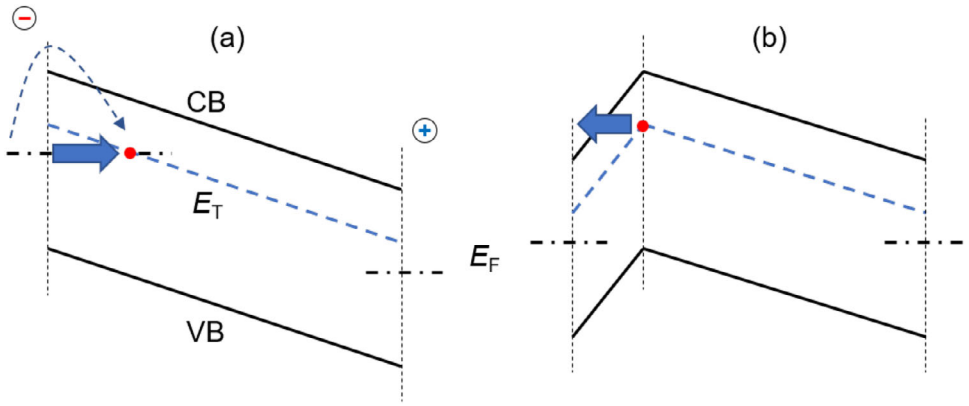

FIGURE 5 | An (anti)ferroelectric material with an electron trap level, E_T. The electron trap can be occupied by charge injection if the electrode is cathodically biased (a). The electric field generated by the trapped charges after removal of the electric field will remove the trapped electrons (b). The mechanism explains the double hysteresis loop of antiferroelectric materials, for which the high-field ferroelectric state is established by charge injection, expected to occur via thermionic emission (dashed blue arrow).

a band gap of 3.7 eV [39], the barrier for electron injection into the conduction band is even higher. Candidates for trap states are hole traps on Pb and electron traps either on Ti, Sn, or Pb [29, 40–42]. Electron trapping on Ti is often discussed for PZT with near morphotropic composition (Ti/Zr ≈ 1) [41, 42], while electron trapping on Pb is indicated by the observation of metallic Pb once the Fermi level at the interface is raised to ≈ 2.45 eV above the valence band maximum in the antiferroelectric Zr-rich compositions [29]. The difference between high and low Zr content PZT is related to the dependence of the electronic structure on the Zr content. For lower Zr content, the electronic states at the conduction band minimum are formed by Ti 3*d* orbitals, while Pb 6*p* dominates for Zr-rich compositions [39]. Sn may also constitute an electron trap, as it can be present as neutral Sn^{4+} or as Sn^{2+}. The electron trap level in PLZST is expected to be close to the Fermi level at the interface to ITO [29], resulting in rather small potential barriers for charge injection into trap states. A rather low electric field may then already result in occupation of trap states, as illustrated in Figure 5a. According to this scenario, occupation of trap states can be easily accomplished. It is mentioned that charge injection is frequently used to explain the leakage currents of dielectric/ferroelectric thin films [23, 24]. The situation for thin films differs from the present case, as much higher electric fields are applied, for which also Schottky barrier lowering by image charge effects has to be taken into account.

Why the injection behavior is different for PLZST having only 2 % different Ti content or why heating from room temperature to 100°C should result in different charge injection are questions, which cannot be answered at present, as details of the charge injection and the nature of the potentially involved trap states are not resolved yet. Defect properties and the electronic structure of antiferroelectric materials are largely unknown. For ferroelectrics, the role of defects is mostly discussed in connection to anion (oxygen) and cation vacancies and their interaction with dopants and domain walls [43, 44]. This cannot constitute a sufficient description as trapped charges, which are well established in ferroelectrics, are not included in this picture (see e.g., [29, 40–42, 45, 46]). The trapped charges will not only affect electrical properties, but they are also strongly changing the defect equilibria and concentrations by modifying the electronic defect reaction [47] and further affect optical properties [45, 48]. A quantification of the role of trap states will require knowledge of their energy levels, which remain to be identified.

4 | Summary and Conclusion

X-ray photoelectron spectroscopy with in situ polarization control is performed on ferroelectric and antiferroelectric Pb-based piezoelectric compounds with thin RuO_2 and ITO top electrodes. Pb 4*f* spectra recorded through the electrodes revealed noticeable differences of binding energy shifts in dependence on the polarity of the applied voltage. Changes in Pb 4*f* binding energy and peak shape are only observed for samples exhibiting ferroelectric polarization hysteresis loops with stable remanent polarization after removal of the applied electric field. The binding energy shifts can be attributed to an imperfect screening of polarization. In contrast, no changes in binding energy are observed for samples exhibiting antiferroelectric polarization hysteresis loops. The absence of binding energy shifts is not explained by perfect screening of polarization, as it is induced by a small variation either of the chemical composition of the sample or measurement temperature.

A quantitative consideration of polarization reveals that the charges present in a few nanometer thick ITO electrode are not sufficient to screen the polarization. If all screening charges remain on the electrode, positive polarization of the ITO electrode should result in a strong suppression of its conductivity and strongly asymmetric polarization hysteresis loops. Such loops are observed with thin ITO electrodes for PMN-PT and $BaTiO_3$ substrates. In contrast, the PZT reference (PIC 151) and the PLZST samples containing 9% or 11% Ti exhibit symmetric polarization loops, indicating that the screening charges are injected into the substrate, at least partially. Measurements of polarization hysteresis loops with thin semiconducting electrodes such as ITO can thus be used to directly access the injection of screening charges. Analysis of the In 3*d* binding energy and peak shape, and of the Pb 4*f* peak shape suggests complete injection of the screening charges for samples exhibiting antiferroelectric hysteresis loops.

The polarization screening by injected charges also explains the reversibility of the field-induced antipolar-polar phase transition. A stable remanent polarization and ferroelectric hysteresis loops may hence require that at least part of the screening charges are not injected from the electrode. So far, it is not clear whether such a relation is fundamental to antiferroelectrics in general or just valid for the specific materials studied. It remains also unclear why only antiferroelectric materials exhibit complete screening by injected charges. This might be connected to differences on the nature and energies of trap states, which are assumed to be involved in the charge injection mechanism.

5 | Method

The interface studies are performed using polycrystalline bulk ceramics of 2 % La-doped $Pb(Zr_{0.75}Sn_{0.25-x}Ti_x)O_3$ with $x = 0.09$ (C09) and $x = 0.11$ (C11) located next to the ferroelectric–antiferroelectric phase transition [49]. The samples are prepared using the conventional solid–state ceramic route with a final sintering step performed at 1250°C. Structural analysis using X-ray diffraction is included in the Supporting Information. It is fully consistent with literature reports [49–56] and does not reveal noticeable changes in structure for unpoled samples C09 and C11. Polarization-electric field ($P - E$) hysteresis loops recorded at room temperature for different compositions and in dependence on temperature are also provided in the Supporting Information. These, as well as strain-field hysteresis loops and dielectric permittivity in dependence on temperature and electric field (both not included in the Supporting Information but available in [57]) confirm the known phase behavior in dependence on composition. In order to obtain fully polarised samples inside the XPS system, where voltages are limited to < 1 kV, the samples are first ground with sandpaper (#1200, #2400, #4000) and then polished with a polishing disk and diamond paste (6,3, 1, $\frac{1}{4}$ μm) to a final thicknesses of $0.12 - 0.16$ mm. For comparison, commercial PIC 151 bulk ceramic pellets (PI ceramics, Lederhose, Germany; composition: $Pb_{0.99}(Zr_{0.45}Ti_{0.47}(Ni_{0.33}Sb_{0.67})_{0.08})O_3$) are used.

For recording polarization hysteresis loops and XPS with applied voltages, the same sample configuration is comparable to that used for studying the electrochemical interface stability [29]. Thin ($3 - 5$ nm) RuO_2 or ITO top electrodes are deposited by magnetron sputtering using the Darmstadt Integrated System for Materials Research (DAISY-MAT) [32]. Prior to electrode deposition, the surface of the pellet is cleaned by annealing in a low pressure oxygen ambient at 400°C for 1 h. The use of oxide electrode materials prohibits interface reactions and island formation [32]. A 50 nm thick Pt film was used as the bottom electrode. After electrode preparation, the samples are mounted on a sectioned sample holder, allowing to apply voltages up to 1000 V between the bottom and top electrode on the sample stage of the XPS system (Physical Electronics PHI 5700, Chanhassan, MN). The top electrode is always grounded during XPS measurement to avoid disturbance of the emitted electrons by the applied field and to ensure a proper binding energy reference. As the conductivity of the electrodes is even sufficient to switch polarization, charging related contributions to the binding energy shifts of the photoelectron spectra can safely be excluded. XP spectra are excited using monochromatic Al Kα radiation providing an overall energy resolution of 0.4 eV as determined from the Gaussian broadening of a sputtered cleaned Ag foil. Spectra were recorded at a 45° emission angle. The shape of the top contact on the sample holder (see Supporting Information), which is designed to prevent that the high voltages (up to 1 kV) applied to the bottom contact are affecting the photoelectron spectra, prevents measurements with higher emission angles, i.e. with lower surface sensitivity, as the X-ray source forms a 90° angle with the electron analyzer axis. Polarization hysteresis loops are recorded on the XPS sample stage with a home made Sawyer-Tower setup. A model 1HVA24-BP1-F high-voltage amplifier (Advanced Energy Industries, Inc., USA), supporting dc voltages up to ±1 kV is used. A 100 Ω series resistor is used when applying constant voltages during XPS measurements to protect the amplifier in case of potential sample breakdown.

Acknowledgements

The presented work was supported by the state of Hesse, Germany, within the LOEWE priority project FLAME (Fermi Level Engineering of Antiferroelectric Materials for Energy Storage and High Voltage Insulation Systems), the German Research Foundation (DFG) within the collaborative research center FLAIR (Fermi level engineering applied to oxide electroceramics), Grant No. 463184206–SFB 1548. P.H. further acknowledges support from the China Scholarship Council (CSC) (Award No. 202106220039). T.R. would like to acknowledge the Slovenian Research and Innovation Agency for funding (research core funding P2-0105 and research project J2-3042).

Open access funding enabled and organized by Projekt DEAL.

Conflicts of Interest

The authors declare no conflicts of interest.

Data Availability Statement

The data that support the findings of this study are openly available in [tudatalib] at https://tudatalib.ulb.tu-darmstadt.de/handle/tudatalib/4970.

References

1. C. A. Randall, Z. Fan, I. Reaney, L.-Q. Chen, and S. Trolier-McKinstry, "Antiferroelectrics: History, Fundamentals, Crystal Chemistry, Crystal Structures, Size Effects, and Applications," *Journal of the American Ceramic Society* 104, no. 8 (2021): 3775–3810.

2. K. M. Rabe, "Antiferroelectricity in Oxides: A Reexamination," in *Functional Metal Oxides: New Science and Novel Applications*, (Eds.: S. B. Ogale, T. V. Venkatesan, M. G. Blamire), (Wiley-VCH, 2013), 221–244.

3. M. Stengel, D. Vanderbilt, and N. A. Spaldin, "Enhancement of Ferroelectricity at Metal–Oxide Interfaces," *Nature Materials* 8 (2009): 392–397.

4. P. Zubko, S. Gariglio, M. Gabay, P. Ghosez, and J.-M. Triscone, "Interface Physics in Complex Oxide Heterostructures," *Annual Review of Condensed Matter Physics* 2 (2011): 141–165.

5. T. Sluka, A. K. Tagantsev, D. Damjanovic, M. Gureev, and N. Setter, "Enhanced Electromechanical Response of Ferroelectrics Due to Charged Domain Walls," *Nature Communications* 3 (2012): 748.

6. J. A. Mundy, J. Schaab, Y. Kumagai, et al., "Functional Electronic Inversion Layers at Ferroelectric Domain Walls," *Nature Materials* 16, no. 6 (2017): 622–627.

7. M. Stengel and N. A. Spaldin, "Origin of the Dielectric Dead Layer in Nanoscale Capacitors," *Nature* 443 (2006): 679–682.

8. M. Stengel, P. Aguado-Puente, N. A. Spaldin, and J. Junquera, "Band Alignment at Metal/Ferroelectric Interfaces: Insights and Artifacts from First Principles," *Physical Review B* 83 (2011): 235112.

9. F. Chen and A. Klein, "Polarization Dependence of Schottky Barrier Heights at Interfaces of Ferroelectrics Determined by Photoelectron Spectroscopy," *Physical Review B* 86 (2012): 094105.

10. J. E. Rault, G. Agnus, T. Maroutian, et al., "Interface Electronic Structure in a Metal/Ferroelectric Heterostructure Under Applied Bias," *Physical Review B* 87 (2013): 155146.

11. E. Kröger, A. Petraru, A. Quer, et al., "In Situ Hard X-Ray Photoemission Spectroscopy of Barrier-Height Control at Metal/PMN-PT Interfaces," *Physical Review B* 93 (2016): 235415.

12. R. Kretschmer and K. Binder, "Surface Effects on Phase Transitions in Ferroelectrics and Dipolar Magnets," *Physical Review B* 20 (1979): 1065–1076.

13. K. Binder, "Surface Effects on Phase Transitions in Ferroelectrics and Antiferroelectrics," *Ferroelectrics* 35, no. 1 (1981): 99–104.

14. M. Grossmann, O. Lohse, D. Bolten, U. Boettger, T. Schneller, and R. Waser, "The Interface Screening Model as Origin of Imprint in $PbZr_xTi_{1-x}O_3$ Thin Films. I. Dopant, Illumination, and Bias Dependence," *Journal of Applied Physics* 92, no. 5 (2002): 2680–2687.

15. M. Grossmann, O. Lohse, D. Bolten, U. Boettger, and R. Waser, "The Interface Screening Model as Origin of Imprint in $PbZr_xTi_{1-x}O_3$ Thin Films. II. Numerical Simulation and Verification," *Journal of Applied Physics* 92, no. 5 (2002): 2688–2696.

16. A. K. Tagantsev and I. A. Stolichnov, "Injection-Controlled Size Effect on Switching of Ferroelectric Thin Films," *Applied Physics Letters* 74, no. 9 (1999): 1326–1328.

17. A. K. Tagantsev, I. Stolichnov, N. Setter, and J. S. Cross, "Nature of Nonlinear Imprint in Ferroelectric Films and Long-Term Prediction of Polarization Loss in Ferroelectric Memories," *Journal of Applied Physics* 96, no. 11 (2004): 6616–6623.

18. A. K. Tagantsev and G. Gerra, "Interface-Induced Phenomena in Polarization Response of Ferroelectric Thin Films," *Journal of Applied Physics* 100, no. 5 (2006): 051607.

19. X. J. Lou, M. Zhang, S. A. T. Redfern, and J. F. Scott, "Fatigue as a Local Phase Decomposition: A Switching-Induced Charge-Injection Model," *Physical Review B* 75, no. 22 (2007): 224104.

20. X. J. Lou, "Why Do Antiferroelectrics Show Higher Fatigue Resistance Than Ferroelectrics Under Bipolar Electrical Cycling?," *Applied Physics Letters* 94, no. 7 (2009): 072901.

21. I. Stolichnov, A. K. Tagantsev, E. L. Colla, and N. Setter, "Cold-Field-Emission Test of the Fatigued State of $Pb(Zr_xTi_{1-x})O_3$ Films," *Applied Physics Letters* 73, no. 1361–1363 (1998): 1361–1363.

22. J. F. M. Cillessen, M. W. J. Prins, and R. M. Wolf, "Thickness Dependence of the Switching Voltage in All-Oxide Ferroelectric Thin-Film Capacitors Prepared by Pulsed Laser Deposition," *Journal of Applied Physics* 81, no. 6 (1997): 2777–2783.

23. G. W. Dietz, M. Schumacher, R. Waser, S. K. Streiffer, C. Basceri, and A. I. Kingon, "Leakage Currents in $Ba_{0.7}Sr_{0.3}TiO_3$ Thin Films for Ultrahigh-Density Dynamic Random Access Memories," *Journal of Applied Physics* 82 (1997): 2359–2364.

24. L. Pintilie, I. Vrejoiu, D. Hesse, G. LeRhun, and M. Alexe, "Ferroelectric Polarization–Leakage Current Relation in High Quality Epitaxial $Pb(Zr,Ti)O_3$ Films," *Physical Review B* 75 (2007): 104103.

25. A. Q. Jiang, H. J. Lee, G. H. Kim, and C. S. Hwang, "The Inlaid Al_2O_3 Tunnel Switch for Ultrathin Ferroelectric Films," *Advanced Materials* 21, no. 28 (2009): 2870–2875.

26. S. Li, Y. Zheng, R. Jakoby, and A. Klein, "Electrically Programmable Bistable Capacitor for High Frequency Applications Based on Charge Storage at the $(Ba,Sr)TiO_3/Al_2O_3$ Interface," *Advanced Functional Materials* 22, no. 22 (2012): 4827–4832.

27. H. W. Park, S. D. Hyun, I. S. Lee, et al., "Polarizing and Depolarizing Charge Injection Through a Thin Dielectric Layer in a Ferroelectric–Dielectric Bilayer," *Nanoscale* 13, no. 4 (2021): 2556–2572.

28. M. Hoffmann, M. Gui, S. Slesazeck, et al., "Intrinsic Nature of Negative Capacitance in Multidomain $Hf_{0.5}Zr_{0.5}O_2$-Based Ferroelectric/Dielectric Heterostructures," *Advanced Functional Materials* 32, no. 2 (2022): 2108494.

29. B. Huang, P. Erhart, T. Yang, and A. Klein, "Electrostatic Boundary Conditions and (Electro)Chemical Interface Stability," *Advanced Materials Interfaces* 10, no. 21 (2023): 2300332.

30. Y. Hermans, A. Klein, K. Ellmer, R. van de Krol, T. Toupance, and W. Jaegermann, "Energy Band Alignment of $BiVO_4$ from Photoelectron Spectroscopy of Solid-State Interfaces," *Journal of Physical Chemistry C* 122 (2018): 20861–20870.

31. A. Klein, C. Körber, A. Wachau, et al., "Surface Potentials of Magnetron Sputtered Transparent Conducting Oxides," *Thin Solid Films* 518 (2009): 1197–1203.

32. A. Klein, "Interface Properties of Dielectric Oxides," *Journal of the American Ceramic Society* 99 (2016): 369–387.

33. F. Chen, R. Schafranek, S. Li, W. Wu, and A. Klein, "Energy Band Alignment Between $Pb(Zr,Ti)O_3$ and High and Low Work Function Conducting Oxides – From Hole to Electron Injection," *Journal of Physics D: Applied Physics* 43 (2010): 295301.

34. A. Klein, A. Frebel, B. Huang, and K. A. Creutz, "Origin and Quantification of the Ultimate Carrier Concentration Limits in In_2O_3 and Sn-Doped In_2O_3," *Physical Review Materials* 8 (2024): 044601.

35. V. M. Fridkin, *Ferroelectric Semiconductors* (Plenum Press, 1980).

36. E. Y. Tsymbal and H. Kohlstedt, "Tunneling Across a Ferroelectric," *Science* 313, no. 5784 (2006): 181–183.

37. Y. Gassenbauer, R. Schafranek, A. Klein, et al., "Surface States, Surface Potentials and Segregation at Surfaces of Tin-Doped In_2O_3," *Physical Review B* 73, no. 24 (2006): 245312.

38. F. Chen, R. Schafranek, A. Wachau, et al., "Barrier Heights, Polarization Switching and Electrical Fatigue in $Pb(Zr,Ti)O_3$ Ceramics with Different Electrodes," *Journal of Applied Physics* 108 (2010): 104106.

39. H. Lee, Y. S. Kang, S.-J. Cho, et al., "Dielectric Functions and Electronic Band Structure of Lead Zirconate Titanate Thin Films," *Journal of Applied Physics* 98, no. 9 (2005): 094108.

40. J. Robertson, W. L. Warren, B. A. Tuttle, D. Dimos, and D. M. Smyth, "Shallow Pb^{3+} Hole Traps in Lead Zirconate Titanate Ferroelectrics," *Applied Physics Letters* 63, no. 11 (1993): 1519–1521.

41. J. Robertson, W. L. Warren, and B. A. Tuttle, "Band States and Shallow Hole Traps in $Pb(Zr,Ti)O_3$ Ferroelectrics," *Journal of Applied Physics* 77, no. 8 (1995): 3975–3980.

42. B. Akkopru-Akgun, T. J. M. Bayer, K. Tsuji, et al., "Leakage Current Characteristics and DC Resistance Degradation Mechanisms in Nb Doped PZT Films," *Journal of Applied Physics* 129, no. 17 (2021): 174102.

43. D. Damjanovic, "Contributions to the Piezoelectric Effect in Ferroelectric Single Crystals and Ceramics," *Journal of the American Ceramic Society* 88, no. 10 (2005): 2663–2676.

44. T. Rojac and D. Damjanovic, "Domain Walls and Defects in Ferroelectric Materials," *Japanese Journal of Applied Physics* 56, no. 10S (2017): 10PA01.

45. N. Bein, B. Kmet, T. Rojac, et al., "Fermi Energy, Electrical Conductivity, and the Energy Gap of $NaNbO_3$," *Physical Review Materials* 6 (2022): 084404.

46. T. Rojac, A. Bencan, G. Drazic, et al., "Domain-Wall Conduction in Ferroelectric $BiFeO_3$ Controlled by Accumulation of Charged Defects," *Nature Materials* 16 (2017): 322.

47. A. Klein, K. Albe, N. Bein, et al., "The Fermi Energy as Common Parameter to Describe Charge Compensation Mechanisms: A Path to

Fermi Level Engineering of Oxide Electroceramics," *Journal of Electroceramics* 51 (2023): 147–177.

48. W. G. Schmidt, M. Albrecht, S. Wippermann, et al., "$LiNbO_3$ Ground- and Excited-State Properties from First-Principles Calculations," *Physical Review B* 77, no. 3 (2008): 035106.

49. D. Berlincourt, H. H. A. Krueger, and B. Jaffe, "Stability of Phases in Modified Lead Zirconate with Variation in Pressure, Electric Field, Temperature and Composition," *Journal of Physics and Chemistry of Solids* 25, no. 7 (1964): 659–674.

50. E. Sawaguchi, "Ferroelectricity Versus Antiferroelectricity in the Solid Solutions of $PbZrO_3$ and $PbTiO_3$," *Journal of the Physical Society of Japan* 8, no. 5 (1953): 615–629.

51. D. Berlincourt, "Transducers Using Forced Transitions Between Ferroelectric and Antiferroelectric States," *IEEE Transactions on Sonics and Ultrasonics* 13, no. 4 (1966): 116–124.

52. J. S. Speck, M. De Graef, A. P. Wilkinson, A. K. Cheetham, and D. R. Clarke, "Hierarchical Domain Structures and In Situ Domain Migration in the Antiferroelectric Ceramic PLSnZT," *Journal of Applied Physics* 73, no. 11 (1993): 7261–7267.

53. C. T. Blue, J. C. Hicks, S. Park, S. Yoshikawa, and L. E. Cross, "In Situ X-Ray Diffraction Study of the Antiferroelectric–Ferroelectric Phase Transition in PLSnZT," *Applied Physics Letters* 68, no. 21 (1996): 2942–2944.

54. S.-E. Park, M.-J. Pan, K. Markowski, S. Yoshikawa, and L. E. Cross, "Electric Field Induced Phase Transition of Antiferroelectric Lead Lanthanum Zirconate Titanate Stannate Ceramics," *Journal of Applied Physics* 82, no. 4 (1997): 1798–1803.

55. F. Zhuo, Q. Li, J. Gao, et al., "Structural Phase Transition, Depolarization and Enhanced Pyroelectric Properties of $(Pb_{1-1.5x}La_x)(Zr_{0.66}Sn_{0.23}Ti_{0.11})O_3$ Solid Solution," *Journal of Materials Chemistry C* 4, no. 29 (2016): 7110.

56. H. Wang, Y. Liu, T. Yang, and S. Zhang, "Ultrahigh Energy-Storage Density in Antiferroelectric Ceramics with Field-Induced Multiphase Transitions," *Advanced Functional Materials* 29, no. 7 (2019): 1807321.

57. B. Huang, "Charges and Charged Defects in Pb-Based Ferro- and Antiferroelectric Ceramics," Ph.D. dissertation, Technical University of Darmstadt; available online at:, https://tuprints.ulb.tu-darmstadt.de/24426/ (2023).

Supporting Information

Additional supporting information can be found online in the Supporting Information section.

Supporting File: admi70362-sup-0001-SuppMat.pdf